The endosperm cavity of wheat grains contains a highly hydrated gel of arabinoxylan

Anne-Laure Chateigner-Boutin, Camille Alvarado, Marie-Françoise Devaux, Sylvie Durand, Loïc Foucat, Audrey Geairon, Florent Grélard, Frédéric Jamme, Hélène Rogniaux, Luc Saulnier, et al.

HAL Id: hal-03149665
https://hal.inrae.fr/hal-03149665v1

Preprint submitted on 23 Feb 2021

Journal Pre-proof

The endosperm cavity of wheat grains contains a highly hydrated gel of arabinoxylan

Anne-Laure Chateigner-Boutin, Camille Alvarado, Marie-Françoise Devaux, Sylvie Durand, Loïc Foucat, Audrey Geairon, Florent Grélard, Frédéric Jamme, Hélène Rogniaux, Luc Saulnier, Fabienne Guillon

Please cite this article as: Chateigner-Boutin A-Laure, Alvarado C, Devaux M-Françoise, Durand S, Foucat L, Geairon A, Grélard F, Jamme F, Rogniaux H, Saulnier L, Guillon F, The endosperm cavity of wheat grains contains a highly hydrated gel of arabinoxylan, *Plant Science* (2021), doi: https://doi.org/10.1016/j.plantsci.2021.110845

This is a PDF file of an article that has undergone enhancements after acceptance, such as the addition of a cover page and metadata, and formatting for readability, but it is not yet the definitive version of record. This version will undergo additional copyediting, typesetting and review before it is published in its final form, but we are providing this version to give early visibility of the article. Please note that, during the production process, errors may be discovered which could affect the content, and all legal disclaimers that apply to the journal pertain.

The endosperm cavity of wheat grains contains a highly hydrated gel of arabinoxylan.

Anne-Laure Chateigner-Boutin [(1)], **Camille Alvarado** [(1)], **Marie-Françoise Devaux** [(1)], **Sylvie Durand (1)**, **Loïc Foucat** [(1)(2)], **Audrey Geairon** [(1)], **Florent Grélard** [(1)(2)], **Frédéric Jamme** [(3)], **Hélène Rogniaux** [(1)(2)], **Luc Saulnier** [(1)], **Fabienne Guillon** [(1)]

[(1)] INRAE, UR BIA, F-44316 Nantes, France

[(2)] INRAE, BIBS facility, F-44316 Nantes, France

[(3)] DISCO beamline, SOLEIL synchrotron, 91192 Gif-sur-Yvette, France

[*]Corresponding author : **Anne-Laure Chateigner-Boutin**

INRAE-BIA-PVPP Rue de la Géraudière BP71627 44316 Nantes Cedex 3 France

anne-laure.chateigner-boutin@inrae.fr

Highlights

- the wheat grain central endosperm cavity is filled with a gel-like structure
- the gel-like structure autofluoresces under UV excitation
- it contains fluorescent, water-absorbing and gel-forming feruloylated arabinoxylans
- high and stable cavity water content suggests a role in regulating grain hydration

Abstracts

Cereal grains provide a substantial part of the calories for humans and animals. The main quality determinants of grains are polysaccharides (mainly starch but also dietary fibers such as

arabinoxylans, mixed-linkage glucans) and proteins synthesized and accumulated during grain development in a specialized storage tissue: the endosperm.

In this study, the composition of a structure localized at the interface of the vascular tissues of the maternal plant and the seed endosperm was investigated. This structure is contained in the endosperm cavity where water and nutrients are transferred to support grain filling. While studying the wheat grain development, the cavity content was found to autofluoresce under UV light excitation. Combining multispectral analysis, Fourier-Transform infrared spectroscopy, immunolabeling and laser-dissection coupled with wet chemistry, we identified in the cavity arabinoxylans and hydroxycinnamic acids. The cavity content forms a "gel" in the developing grain, which persists in dry mature grain and during subsequent imbibition. Microscopic magnetic resonance imaging revealed that the gel is highly hydrated.

Our results suggest that arabinoxylans are synthesized by the nucellar epidermis, released in the cavity where they form a highly hydrated gel which might contribute to regulate grain hydration.

Keywords

Cereal grain, arabinoxylan, hydroxycinnamic acids, endosperm cavity

Abbreviations

AX: arabinoxylan; °DAF: Celsius degrees per day after flowering; FT-IR: Fourier Transform-InfraRed; µMRI: microscopic magnetic resonance imaging; HPLC-DAD: HPLC combined with UV diode array detection.

1. Introduction

Wheat is a major crop providing a substantial part of human and animal diet calories. The main biochemical components of wheat grains are starch, proteins, lipids and non-starch polysaccharides that all contribute to wheat nutritional properties and affect its processing quality [1].

As other cereal grains, the wheat caryopsis contains several tissues: several layers of outer tissues (pericarp, seed coat, nucellar epidermis), an embryo and a storage tissue named endosperm (**Fig. 1**). These tissues are the results of a precise programmed development, which takes place following fertilization [2]. Grain development is classically divided into the early (lag) phase, the filling phase and the maturation phase. After anthesis, the wheat grain mainly consists of the pericarp whose cells first divide and then extend. In the seed, the nucellus degenerates and the endosperm and embryo develop. The endosperm forms from free nuclei that divide and subsequently produce cell walls (cellularization). These endosperm cells then undergo cell division and cell differentiation into the aleurone layer, the modified aleurone (or aleurone transfer cells) and starchy endosperm cells which switch their metabolism to accumulate storage compounds. In parallel, the outer layers undergo drastic changes. The parenchyma cells of the pericarp are eliminated through a developmental programmed cell death. Other living outer tissues active in the early development phase collapse at the end of the development. This is the case for the photosynthetically active inner pericarp, the seed coat, and nucellar epidermis. At the end of the filling phase, the grain enters the maturation phase and desiccates [3-4].

During the stage of grain filling, precursors of storage compounds are transported from the wheat mother plant to the endosperm via the vascular tissues located in the pericarp in the grain ventral region [5]. This region forms a crease, which is particularly deep in wheat (and in barley) when compared to other cereals [6]. From the maternal vascular tissue, the route to the endosperm passes through the chalaza, the nucellar projection cells, towards the aleurone transfer cells and starchy endosperm cells [7] (**Fig. 1**). In wheat, as in barley, the nucellar projection cells and the endosperm transfer cells are separated by a cavity named endosperm cavity where nutrients and water are released [7-9]. Subsequently, the nutrients are captured by the aleurone transfer cells [10], which exhibit specific features such as thickened cell walls and wall ingrowths facilitating nutrient uptake [7]. A recent study in barley revealed the importance of the integrity of the endosperm cavity and transfer cells for grain development and filling [11].

The wheat endosperm cavity and its content named cavity "sap" were studied in the eighties/nineties [10, 12-14] and more recently in barley [15-16]. It was described to contain sucrose, glucose, amino acids, potassium, and fructans (soluble fructose-based oligosaccharides) [12-13]. However, Fisher and Gifford [13] hypothesized that the cavity also contains high molecular weight compounds that cause the cavity content to appear viscous.

3

While studying the histology and cell wall composition of developing wheat grains with respect to grain growth [17-20], the crease region has captured our interest. Micro-computed X-Ray tomography revealed that the internal compartment comprising the endosperm, nucellar epidermis and seed coat is entirely filled from anthesis to the grain filling stage [20]. A gel-like structure was observed in the endosperm cavity of developing wheat grains, and this structure exhibited autofluorescence properties.

The objective of this work was to study the biochemical composition of the endosperm cavity content and its evolution during grain development, to identify the high molecular compound responsible for its gel-like appearance and to explore its biological function.

2. Material and methods

2.1. Plant material and growth conditions

Growth of the wheat (*Triticum aestivum L.* cv Recital) plants and grain harvesting was carried out as described in [21]. Briefly, the plants were grown in a controlled glasshouse at INRAE Le Rheu (France), individual spikes were tagged at flowering and stages were assessed by the thermal time method (cumulated average temperature in Celsius degrees per day after flowering, °DAF). The two basal grains of the spike middle spikelets were harvested at different stages of development.

2.2. Sample preparation, sectioning and microscopy acquisitions

Wheat grain samples were prepared and imaged using different methods. The procedures of sample preparation, sectioning and acquisition settings are indicated in **Table 1** with references.

For immunolabelings, the antibody used was anti-AX1 which targets cell wall arabinoxylans [22]. The procedure was described in [23]. Control experiments were performed without primary antibodies.

The grain samples used for staining and immunodetection were embedded, for all other image acquisitions, freshly harvested grain samples were directly frozen and cut immediately without further preparation.

4

For confocal imaging and fluorescence profile analyses, sections were placed on a quartz slide and observed mounted in air using a confocal laser-scanning system (A1, Nikon). The microscope was equipped with a spectral detector unit. At the chosen magnification, the field of view was 312 × 312 μm and images were digitized as matrix of 512 × 512 pixels with a pixel size of 0.61 × 0.61 μm. Hyperspectral images were recorded by collecting emitted light from 414 to 704 nm for UV excitation with a 10 nm step between spectral variables. A dichroic mirror was used to filter the excitation wavelengths. Three grains were imaged per development stage. Emission profiles of gels and nucellus epidermis cell walls were directly extracted from the images using the Nikon software. For the three grains per stage, on one image, several regions within the gel and within the nucellar epidermis cell walls were selected. Average emission spectra were calculated by integrating the results for the regions and the three grains.

For deep UV autofluorescence multispectral acquisitions, the full field so-called TELEMOS microscope of the DISCO beamline at the synchrotron SOLEIL was used [24,25]. Deep UV excitation was set to 280 nm and fluorescence emission was recorded using 9 different band-pass filters with optimized acquisition time (**Table 1**). The samples were placed between quartz lamella (R52-5000, ESCO Optics). They included grain cryo-sections and reference samples (commercial ferulic and *p*-coumaric acid, purified ferulic acid ester-linked to arabinose, gluten, and lignin from maize stem). The field of view was 292 x 292 μm^2 and pixel size 0.2768 μm. Images were background subtracted and processed to compensate illumination inhomogeneity as in [26]. Fluorescence emission was valued based on the grey scale intensity of pixels. Pseudospectra were obtained from the multispectral images: pixels were manually selected in targeted structures and their intensity profile was extracted using a home-made function in Matlab [27].

2.3 Fourier Transform-InfraRed (FT-IR) spectroscopy

Cryo-sections (transverse, 30 μm thickness) of fresh grains were collected on ZnS windows. IR micro-spectroscopy was performed on a Tensor 27 (Bruker) spectrometer equipped with a Hyperion 2000 microscope (Bruker). The detector of the IR microscope was a liquid nitrogen cooled mercury cadmium telluride detector. Bright-field images were obtained using a Sony camera (Exwave HAD, SSC-DC80P). IR spectra were collected in transmission mode between 2000-700 cm^{-1} at a resolution of 8 cm^{-1} using a 15X objective (NA 0.4), using a double path single masking aperture size varying from 25x25 to 50x50 μm depending on the cavity shape. IR spectra resulted from the co-addition of

700 scans for the background and 500 scans for the samples. Spectra were baseline corrected and unit vector normalized using Opus software 7.5. The second derivative data were obtained using Norris gap algorithm (Unscrambler software 10.1, Camo). Two series of analyses were conducted on grains harvested from wheat plants grown in two different years and for both years, 3 grains were analyzed per stage. The arabinoxylan fractions with different arabinose-to-xylose ratios (A/X, 0.41 and 0.67) used as reference were obtained as described in [28].

2.4 Laser microdissection and biochemical analysis

Fourty grains coming from 10 spikes were cryo-sectioned for two stages (350°DAF and 650°DAF). Cryo-sections (100 µm thick) were placed on dissection slides (16x45 mm with 1.4 µm membrane in polyethylene terephthalate 11505151, LEICA). Laser assisted microdissection was carried out using a Laser assisted microdissecter LMD 7000 (LEICA). The sections were visualized in bright-field conditions. Parameters were: objective x10, power 43, opening 21, speed 37, point-to-point mode. The dissected regions were collected in PCR tubes in a drop of water and stored at -20°C.

Ester-linked phenolic compounds were analyzed after mild alkaline hydrolysis essentially as described in [29]. 150 µL of 1 N NaOH were added to the sections and the reaction mixture was incubated overnight at room temperature. The tubes were centrifuged to discard the dissection membranes. The reaction mixture was then acidified with 35 µL of 6 M HCL. After centrifugation (1500 g, 10 min), the supernatant was deposited onto a solid-phase extraction cartridge (Waters Sep-Pak Plus Short tC18 cartridges) pre-conditioned before use. Washes and elution were conducted with 1 mL solutions. The samples were filtrated (0.45 µm) and concentrated three times using a concentrator SpeedVac Savant (Thermo Scientific) and then analyzed by HPLC combined with UV diode array detection (HPLC-DAD). The samples (2 µl) were injected onto a RP18 (Macherey Nagel 2x50 mm 2.7 µm particle size, Nucleoshell RP18plus) column with a flow rate of 0.3 ml.min^{-1}. The eluents were 0.1 % formic acid in water (A) and 0.1 % formic acid in acetonitrile (B), and the gradient was: 0–3 min, 8 % B; 3-20 min increase to 20 % B, 20-23 min 20 % B; 23-24 min increase to 60 % B; 24-26 min decrease to 8 % B; 26-28 min 8 % B. Peaks were assigned from the 320 nm DAD chromatograms according to their retention time by comparison with well-characterized samples (pure aleurone layer, wheat and maize bran) and according to their UV absorption spectra [30].

2.5 Microscopic Magnetic Resonance Imaging (μMRI)

MRI experiments were carried out at room temperature on a Bruker AVANCE III 400 MHz NMR spectrometer equipped with a 9 Tesla/89 mm vertical-bore superconducting magnet and micro-imaging accessory. Individual grains were placed vertically in a homemade Teflon holder incorporating a capillary (inner diameter, 1 mm) filled with doped water for NMR signal amplitude normalization purpose. Proton density images were acquired using multi-slice gradient echo pulse sequence. A 30° excitation pulse (0.43 ms length; 3 kHz bandwidth) was used and the echo time was 1.2 ms. Repetition time of 1 s was sufficient for full relaxation of the magnetization. All transverse 2D images had an acquisition matrix size of 100×100, with a slice thickness of 0.5 mm. Depending on grain dimensions, the field of view was 5×5 mm, 6×6 mm and 6.45×6.45 mm for 250, 850 and 650 °DAF, respectively, resulting in 2D in-plane pixel sizes of 50×50 μm, 60×60 μm and 64.5×64.5 μm. Fourteen to sixteen contiguous slices were acquired to cover the whole grain. The number of averages was 72 for a total acquisition time of 2 h per grain.

Four grains were analyzed by μMRI per development stage. The global water content of grains harvested at the same time than those analyzed by μMRI was determined on minimum 12 grains per stage. Grains were weighed immediately after harvesting, then oven-dried (60 °C for 48 h) and weighed afterwards to deduce the water content.

Three quantitative criteria were estimated from MRI images: (1) the water content of the grain, (2) the water content of the cavity, and (3) the volume of the cavity. In order to obtain these measurements, each component was extracted by image segmentation. First, denoising was achieved by a non-local means method suited to MRI images [31]. The grain and the cavity were segmented by a region growing algorithm with a manually selected seed and threshold. The water content of a segmented component was determined by its average intensity relative to the average intensity of the water-filled capillary. The volume (in mm³) was estimated by the total number of voxels in a segmented component multiplied by the voxel size.

3. Results and discussion

3.1 The endosperm cavity of the wheat grain contains a "gel-like" structure that autofluoresces upon UV excitation.

In our studies of wheat grain development, we have imaged numerous sections of wheat grains at different stages [17-19, 23, 32, 33]. During the course of these studies, the endosperm cavity raised our attention. Indeed, the grain cavity content appears like a gel (**Fig. 1**). Upon grain sectioning, the contents of the cavity do not leak but remain in place. Microcapillar tubes and pipettes with small diameter tips (300 nm) were used to try and aspirate the cavity content for analysis, but these attempts failed. All these observations suggest that the content of the cavity is viscous as described by Fisher and Gifford [13].

The "gel" is visible on grain sections from the onset of grain filling (around 200°DAF for Recital; [18]) to maturity, and in rehydrated mature grains (**Fig. S1**).

We conducted several studies on the fluorescence properties of wheat grain tissues [19, 27] in which we noticed another remarkable feature of the cavity content: it appeared to fluoresce under UV excitation. Examples of fluorescence imaging of wheat grain sections is given in **Fig. S1**. The cavity content fluoresces although less than other grain tissues. The fluorescence properties of the "gel" were studied using multi/hyperspectral analysis and compared to that of other grain tissues. Analysis of the intensity profiles confirmed that upon excitation in UV the "gel" fluoresces with less intensity than its surrounding tissues (**Fig. 2**). The fluorescence intensity of "gels" from grains harvested at different stages of development increased from 250°DAF to 750°DAF (**Fig. 2A**).

Among the compounds known to autofluoresce in the wheat grain, there are hydroxycinnamic acids (ferulic and *p*-coumaric acids). Hydroxycinnamic acids have an absorption/excitability maximum below 350 nm [26], but conventional microscopes are limited in this range with 350 nm cut-off. We decided to take advantage of the sensitivity of synchrotron deep UV microscopy to compare the fluorescence profile of the "gel" at one stage with that of autofluorescent compounds known to be present in the wheat grain. It exhibits two main emission peaks at 370-410 nm and 420-480 nm similar to that obtained for the walls of the nucellar epidermis and from ferulic acid ester-linked to arabinose (**Fig. 2B**). Ferulic acid is linked to several compounds including the arabinosyl residues of arabinoxylans (AX), a major class of polysaccharide present in cell walls of cereal grains [18,34].

3.2 The endosperm cavity contains arabinoxylans and hydroxycinnamic acids which may form a gel

8

In the literature, the endosperm cavity content of the wheat grain is reported to be composed of sucrose, glucose, amino acids, and fructans [12, 13]. None of these compounds fluoresces under UV excitation. In order to identify the fluorescent compound in the cavity, the cavity content was laser-dissected without touching the surrounding tissues and analyzed. Fluorescence profiles suggested the presence of ester-linked hydroxycinnamic acids, therefore the dissected "gel" was submitted to alkaline hydrolysis to break ester-linkages and the released compounds were analyzed by HPLC with UV detection (**Fig. 3**). The chromatograms were compared with those obtained for well-characterized samples and a negative control without grain sections to discard contaminant peaks due to the membrane used in the laser dissection process. In the "gel" samples, peaks corresponding to ferulic, and *p*-coumaric acids were identified (**Fig. 3**). On investigated samples, the peak for ferulic acid has a more important area than the one corresponding to *p*-coumaric. Peaks corresponding to ferulic acid dimers were also observed. These structures cross-link AX chains in cereal grain cell walls [34].

Fisher and Gifford [13] estimated that a yet-to be identified compound would be responsible to the cavity content viscous appearance. AX is known to have gelling properties [35, 36]. We therefore investigated the possibility that the cavity "gel" contains AX.

FT-IR is a method suitable to detect and identify polysaccharides in plant tissues and was already used to study AX in wheat grains [17, 37, 38]. FT-IR analysis was conducted on cryo-sections of grains harvested at several development stages. The Bright-field camera coupled to the spectrometer allowed to target specifically the cavity content.

As for grain tissues, the cavity content comprises several compounds; therefore, the recorded spectra correspond to that of a mix of individual spectra. Different types of spectra were collected in the cavity "gel" and compared with reference spectra (**Fig. 4A**). On some spectra, a starch-specific peak (930 cm^{-1}) and protein-specific signatures were recorded (amide I absorption bands around 1645 cm^{-1} (C=O and C-N) and amide II assignment at 1540 cm^{-1} (C-N, N-H)). On all samples, typical spectra of AX were detected (**Fig. 4A, B**). The band around 1041 cm^{-1} with a shoulder at 990 cm^{-1} assigned to C-C and C-O stretching modes of polysaccharides are typical bands of AX [38]. The 1160 cm^{-1} band is assigned to the C-O-C stretching mode of glycosidic linkages and the peak at about 898 cm^{-1} corresponds to the β(1-4) configuration of the xylan chain.

9

The structure of AX varies according to the wheat grain tissue and the development stage. This concerns the number of arabinosyl residues on the xylan backbone (degree of substitution with arabinose) and the number of hydroxycinnamic acids residues (ferulic and *p*-coumaric acid) ester-linked to the arabinose [18, 37]. Relatively strong absorption bands at 1160 cm^{-1} and 990 cm^{-1}, and an absorption peak at 985 cm^{-1}, highlighted on the second derivative spectra (**Fig. 4C**), were previously described as marker of a relatively low degree of substitution with arabinose [39]. The aromatic skeletal vibration at about 1590 and 1515 cm^{-1} associated with bands at about 810 and 850 cm^{-1} (out of plane C-H bending) was assigned to ferulic acid ester [40, 41]. Thus, when comparing with reference spectra of AX, the AX FT-IR signal in the wheat cavity corresponded to AX with a relatively low level of substitution with arabinose and with ester-linked ferulic acid.

Only subtle variations were observed in the FT-IR AX spectra between development stages and mainly at late stages.

Among the reported favorable factors for the AX gelation, there are a high content of ferulic acid, a high molecular weight/hydrodynamic volume, and a low-substituted xylan backbone [35, 42, 43]. The gelation of feruloylated AXs occurs via covalent cross-links of AX chains due to oxidative coupling of ferulic acid residues [44] resulting in the occurrence of ferulate dimers. The cavity AX has a low-substitution level with arabinose, it contains ferulic acid probably ester-linked to AX chains, and ferulate dimers. These results suggest that cavity AXs features are favorable for AX gelation.

3.3 Origins of the AX present in the gel

In order to identify the tissue origin of the cavity AX, immunolabeling experiments were carried out on sections of grains harvested at different stages of development from flowering (0°DAF) to the onset of grain filling (200°DAF) with an antibody targeting AX. Anti-AX1 recognizes xylan and tolerates arabinose substitution [22].

In wheat ovary at flowering and at 60°DAF, signals were observed in the cell walls of vascular cells and of some cells in the developing nucellar projection (**Fig. 5)**. At 90°DAF the cell wall of the nucellar epidermis in contact with the endosperm appeared labeled. There is a clear polarity in the labeling since only one of the periclinal cell walls reacted with anti-AX1 at this stage (**Fig. 5**). From 110 °DAF, one cell layer of the nucellar projection is particularly labeled (**Fig. 5**). Cell walls of the endosperm transfer cells also reacted with anti-AX1 from this stage. At 200°DAF, the anti-AX1 labeling

10

of the nucellar epidermis is detected in all cell walls of this cell layer. The anti-AX1 antibody positively labeled the "gel" present inside the cavity (**Fig. 5** and **Fig. 6**). Positive labeling was also observed inside cells of the nucellar epidermis in Golgi apparatus and vesicles in the different regions of the grain, and in the apoplast between the nucellar epidermis and the endosperm **(Fig. 6).**

Considering the temporal coincidence between the labeling of the nucellar epidermis and that of the cavity content, considering the proximity of both structures, the intensity of the labeling of the nucellar epidermis and the high vesicular activity apparently associated, it is likely that the nucellar epidermis is the tissue that produces the AX of the cavity.

3.4 The cavity gel is highly hydrated even at late development stages

AX is a structural polysaccharide with major function in the cell wall architecture of cereal grains. In addition, this polysaccharide has gel-forming properties (as mentioned earlier in the text) and high water-binding capacity [36, 45]. The hydration properties of AX depend of the arabinose distribution on the xylan backbone. Films made with low substituted AXs absorb slightly more water than with highly substituted AXs [46]. Cell wall AXs were also suggested to be involved in the modulation of water diffusion in the wheat grain [47-49]. One of the hypothetical function of AX in the cavity might be to maintain hydration.

We therefore studied water level and water distribution in wheat grains at three stages of development. Global water content for the stages were 75 ± 1 % at 250°DAF (grain filling), 51 ± 2 % at 650°DAF (end of filling), 40 ± 1 % at 850°DAF (desiccation stage). Microscopic MRI experiments were conducted using multislice acquisitions along the grain longitudinal axis to cover the entire grain and allow the visualization of water distribution in the different tissues and regions. Variations were observed between the three stages **(Fig. 7).** A high NMR signal was obtained in the endosperm at 250°DAF and lower signal at 850°DAF. Local variations were highlighted. An intense NMR signal signifying high water content was obtained in the vascular bundle of the pericarp responsible for the grain water supply and in the endosperm cavity for the three stages (**Fig. 7**). By normalization to the water reference signal, the water content of the cavity was estimated to be 87 ± 3 %, whatever the stage and whatever the volume of the cavity (the cavity volume was estimated to be 0.57 ± 0.13 mm^3, 2.34 ± 0.47 mm^3 and 0.62 ± 0.11 mm^3 at 250, 650 and 850°DAF, respectively).

Therefore, the hydration level of the cavity content is high, it is maintained at the same level from the filling stage to the desiccation stage although the grain water level drops at the desiccation stage [50].

Conclusion:

Our study of the wheat endosperm cavity confirmed that it is filled with a gel-like structure. In addition to the compounds already known to be present in the cavity, we showed the presence of AX and hydroxycinnamic acids, which are likely involved in the gel-like appearance of the cavity content. We also showed that the cavity content stays highly hydrated through the grain development and maturation. To address the biological significance of the cavity AX, mutants or variants altered in AX will be explored.

Declaration of interests

The authors declare that they have no known competing financial interests or personal relationships that could have appeared to influence the work reported in this paper.

References

[1] P.R. Shewry, Wheat, J. Exp. Bot. 60 (2009) 1537–1553.

[2] T. Evers, S. Millar, Cereal grain structure and development: some implications for quality, J. Cereal Sci. 36 (2002) 261-284.

[3] F. Xiong, X.R. Yu, L. Zhou, F. Wang, A.S. Xiong, Structural and physiological characterization during wheat pericarp development, Plant Cell Rep. 32 (2013) 1309-1320.

[4] P. Sabelli, B. Larkins, The Development of Endosperm in Grasses, Plant Physiology 149 (2009) 14-26.

[5] S. Lingle, P. Chevalier, Development of the vascular tissue of the wheat and barley caryopsis as related to the rate and duration of grain filling, Crop Science 25 (1985) 123-128.

[6] P. Hands, S. Kourmpetli, D. Sharples, R. Harris, S. Drea, Analysis of grain characters in temperate grasses reveals distinctive patterns of endosperm organization associated with grain shape, J. Exp. Bot. 63 (2012) 6253-6266.

[7] Y. Xurun, C. Xinyu, Z. Liang, Z. Jing, Y. Heng, S. Shanshan, X. Fei, W. Zhong, Structural development of wheat nutrient transfer tissues and their relationships with filial tissues development, Protoplasma 252 (2015) 605–617.

[8] J. Thiel, Development of endosperm transfer cells in barley, Front. Plant Sci. 5 (2014):108. doi: 10.3389/fpls

[9] Y. Zheng, Z. Wang, Contrast observation and investigation of wheat endosperm transfer cells and nucellar projection transfer cells, Plant Cell Rep. 30 (2011) 1281–1288.

[10] T.D. Ugalde, C.F. Jenner, Route of substrate movement into wheat endosperm. II. Amino acids, Aust. J. Plant Physiol. 17 (1990) 693–704.

[11] W.L. Lim, H.M. Collins, C.S Byrt, J. Lahnstein, N.J. Shirley, M.K. Aubert, M.R.Tucker, M. Peukert, A. Matros, R.A. Burton, Overexpression of HvCslF6 in barley grain alters carbohydrate partitioning plus transfer tissue and endosperm development, J. Exp. Bot. 71 (2020) 138-153.

[12] D. Fisher, R. Gifford, Accumulation and conversion of sugars by developing wheat grains: VI. Gradients along the transport pathway from the peduncle to the endosperm cavity during grain filling, Plant Physiol. 82 (1986) 1024-1030.

[13] D. Fisher, R. Gifford, Accumulation and conversion of sugars by developing wheat grains: VII. Effect of changes in sieve tube and endosperm cavity sap concentrations on the grain filling rate, Plant Physiol. 84 (1987) 341-437.

[14] N. Wang, D.B. Fisher, Sucrose Release into the Endosperm Cavity of Wheat Grains Apparently Occurs by Facilitated Diffusion across the Nucellar Cell Membranes, Plant Physiol. 109 (1995) 579-585.

[15] M. Peukert, J. Thiel, D. Peshev, W. Weschke, W. Van den Ende, H. Mock, A. Matros, Spatio-temporal dynamics of fructan metabolism in developing barley grains, Plant Cell 26 (2014) 3728-3744.

[16] M. Peukert, J. Thiel, H. Mock, D. Marko, W. Weschke, A. Matros, Spatiotemporal dynamics of oligofructan metabolism and suggested functions in developing cereal grains. Front. Plant Sci. (2016) 6. DOI 10.3389/fpls.2015.01245.

[17] P. Robert, F. Jamme, C. Barron, B. Bouchet, L. Saulnier, P. Dumas, F. Guillon, Change in wall composition of transfer and aleurone cells during wheat grain development, Planta 233 (2011) 393-406.

[18] A.L. Chateigner-Boutin, C. Lapierre, C. Alvarado, A. Yoshinaga, C. Barron, B. Bouchet, B Bakan, L. Saulnier, M. Devaux, C. Girousse, F. Guillon, Ferulate and lignin cross-links increase in cell walls of wheat grain outer layers during late development, Plant Sci. 276 (2018) 199-207.

[19] M. Ghaffari, A.L. Chateigner-Boutin, F. Guillon, M.F. Devaux, H. Abdollahi, L. Duponchel, Multi-excitation hyperspectral autofluorescence imaging for the exploration of biological samples, Anal. Chim. Acta 1062 (2019) 47-59.

[20] T. Le, C. Alvarado, C. Girousse, D. Legland, A.L. Chateigner-Boutin, Use of X-ray micro computed tomography imaging to analyze the morphology of wheat grain through its development, Plant Methods 15 (2019). DOI: 10.1186/s13007-019-0468-y.

[21] Y. Verhertbruggen, A. Bouder, J. Vigouroux, C. Alvarado, A. Geairon, F. Guillon, M.D. Wilkinson, F. Stritt, M. Pauly, M.Y. Lee, J.C. Mortimer, H.V. Scheller, R.A.C. Mitchell, C. Voiniciuc, L. Saulnier, A.L. Chateigner-Boutin, The TaCslA12 gene expressed in the wheat grain endosperm synthesizes wheat-like mannan when expressed in yeast and Arabidopsis, Plant Sci. (2021). DOI:10.1016/j.plantsci.2020.110693

[22] F. Guillon, O. Tranquet, L. Quillien, J.P. Utille, J.J. Ordaz Ortiz, L. Saulnier, Generation of polyclonal and monoclonal antibodies against arabinoxylans and their use for immunocytochemical location of arabinoxylans in cell walls of endosperm of wheat, J. Cereal Sci. 40 (2004) 167-182.

[23] A.L. Chateigner-Boutin, B. Bouchet, C. Alvarado, B. Bakan, F. Guillon, The wheat grain contains pectic domains exhibiting specific spatial and development-associated distribution, PLoS One 9 (2014) e89620. DOI:10.1371/journal.pone.0089620.

[24] F. Jamme, S. Villette, A. Giuliani, V. Rouam, F. Wien, B. Lagarde, M. Réfrégiers, Synchrotron UV fluorescence microscopy uncovers new probes in cells and tissues, Microsc. Microanal. (2010) DOI:10.1017/S1431927610093852.

[25] F. Jamme, S. Kascakova, S. Villette, F. Allouche, S. Pallu, V. Rouam, Réfrégiers M, Deep UV autofluorescence microscopy for cell biology and tissue histology, Biol. Cell 105 (2013) 277–288. DOI: 10.1111/boc.201200075.

[26] K. Vidot, M.F. Devaux, C. Alvarado, S. Guyot, F. Jamme, C. Gaillard, R. Siret, M. Lahaye, Phenolic distribution in apple epidermal and outer cortex tissue by multispectral deep-UV autofluorescence cryo-imaging, Plant Sci. 283 (2019) 51-59.

[27] M. Corcel, M.F. Devaux, F. Guillon, C. Barron, Comparison of UV and visible autofluorescence of wheat grain tissues in macroscopic images of cross-sections and particles, Comput. Electron. Agr. 127 (2016) 281-288.

[28] G. Dervilly, L. Saulnier, P. Roger, J.-F. Thibault, Isolation of homogeneous fractions from wheat water-soluble arabinoxylans. Influence of the structure on their macromolecular characteristics, J. Agric. Food Chem. 48 (2000) 270-278.

[29] S. Ho-Yue-Kuang, C. Alvarado, S. Antelme, B. Bouchet, L. Cezard, P. Le Bris, F. Legee, A. Maia-Grondard, A. Yoshinaga, L. Saulnier, F. Guillon, R. Sibout, C. Lapierre, A.L. Chateigner-Boutin, Mutation in Brachypodium caffeic acid O-methyltransferase 6 alters stem and grain lignins and improves straw saccharification without deteriorating grain quality, J. Exp. Bot. 67 (2016) 227-237.

[30] K.W. Waldron, A.J. Parr, A. Ng, J. Ralph, Cell wall esterified phenolic dimers: identification and quantification by reverse phase high performance liquid chromatography and diode array detection, Phytochem. Anal. 7 (1996) 305–312.

[31] N. Wiest-Daesslé, S. Prima, P. Coupé, S.P. Morrissey, C. Barillot, Rician noise removal by non-local means filtering for low signal-to-noise ratio MRI: applications to DT-MRI, in: medical image computing and computer-assisted intervention, MICCAI 2008, Springer Berlin Heidelberg, 2008, pp. 171-179.

[32] S. Philippe, O. Tranquet, J.P. Utille, L. Saulnier, F. Guillon, Investigation of ferulate deposition in endosperm cell walls of mature and developing wheat grains by using a polyclonal antibody, Planta 225 (2007) 1287-1299.

[33] A.L. Chateigner-Boutin, M. Suliman, B. Bouchet, C. Alvarado, V. Lollier, H. Rogniaux, F. Guillon, C. Larré. Endomembrane proteomics reveals putative enzymes involved in cell wall metabolism in wheat grain outer layers, J. Exp. Bot. 66 (2015) 2649-2658.

[34] C. Barron, A. Surget, X. Rouau, Relative amounts of tissues in mature wheat (*Triticum aestivum* L.) grain and their carbohydrate and phenolic acid composition, J. Cereal Sci. 45 (2007) 88-96.

[35] M. Izydorczyk, C. Biliaderis, Cereal arabinoxylans: Advances in structure and physicochemical properties. Carbohydr. Pol. 28 (1995) 33-48.

[36] L. Saulnier, F. Guillon, P.E. Sado, A.L. Chateigner-Boutin, X. Rouau, Plant Cell Wall Polysaccharides in Storage Organs: Xylans (Food Applications), in: Reedijk, J. (Ed.) Elsevier Reference Module in Chemistry, Molecular Sciences and Chemical Engineering, Waltham, MA: Elsevier, 11-Sep-13 doi: 10.1016/B978-0-12-409547-2.01493-1 (2013).

[37] S. Philippe, P. Robert, C. Barron, L. Saulnier, F. Guillon, Deposition of cell wall polysaccharides in wheat endosperm during grain development: fourier transform-infrared microspectroscopy study, J. Agric. Food Chem. 54 (2006) 2303–2308.

[38] F. Jamme, P. Robert, B. Bouchet, L. Saulnier, P. Dumas, F. Guillon, Aleurone cell walls of wheat grain: high spatial resolution investigation using synchrotron infrared microspectroscopy, Appl. Spectrosc. 62 (2008) 895-900.

[39] P. Robert, M. Marquis, C. Barron, F. Guillon, L. Saulnier, FT-IR investigation of cell wall polysaccharides from cereal grains. Arabinoxylan infrared assignment, J. Agric. Food Chem. 53 (2005) 7014-7018.

[40] S. Sebastian, N. Sundaraganesan, S. Manoharan, Molecular structure, spectroscopic studies and first-order molecular hyperpolarizabilities of ferulic acid by density functional study, Spectrochim. Acta A 74 (2009) 312-323.

[41] R. Chazal, P. Robert, S. Durand, M.F. Devaux, L. Saulnier, C. Lapierre, F. Guillon, Investigating lignin key features in maize lignocelluloses using infrared spectroscopy, Appl. Spectrosc. 68 (2014) 1342-1347.

[42] O. Rattan O, M.S. Izydorczyk, C.G. Biliaderis, Structure and rheological behaviour of arabinoxylans from Canadian bread wheat flours, Lebenson Wiss. Technol. 27 (1994) 550–555.

[43] G. Dervilly-Pinel, L. Rimsten, L. Saulnier, R. Andersson, P. Aman, Water-extractable arabinoxylan from pearled flours of wheat, barley, rye and triticale. Evidence for the presence of ferulic acid dimers and their involvement in gel formation, J. Cereal Sci. 34 (2001) 207-214.

[44] E. Carvajal-Millan, V. Landillon, M. Morel, X. Rouau, J. Doublier, V. Micard, Arabinoxylan gels: Impact of the feruloylation degree on their structure and properties, Biomacromolecules 6 (2005) 309-317.

[45] M. Bonnand-Ducasse, G.Della Valle, J. Lefebvre, L. Saulnier, Effect of wheat dietary fibres on bread dough development and rheological properties, J. Cereal Sci. 52 (2010) 200-206.

[46] R. Ying, C. Rondeau-Mouro, C. Barron, F. Mabille, A. Perronnet, L. Saulnier, Hydration and mechanical properties of arabinoxylans and β-D-glucans films, Carbohydr. Pol. 96 (2013) 31-38.

[47] M. Fanuel, D. Ropartz, F. Guillon, L. Saulnier, H. Rogniaux, Distribution of cell wall hemicelluloses in the wheat grain endosperm: a 3D perspective, Planta 248 (2018) 1505-1513.

[48] R. Ying, T. Li, C. Wu, M. Huang, Role of aleurone cell walls in water diffusion and distribution within cereal grains, J. Cereal Sci. 93 (2020) 102952 doi.org/10.1016/j.jcs.2020.102952.

[49] X. Gao, R. Ying, D. Zhao, J. Zhu, Variation in cell wall structure and composition of wheat grain based on geography and regulatory effect of cell wall on water mobility, Funct. Plant Biol. 47 (2020) . 840-852

[50] H. Neghliz, H. Cochard, N. Brunel, P. Martre, Ear rachis xylem occlusion and associated loss in hydraulic conductance coincide with the end of grain filling for wheat, Front. Plant Sci. 7 (2016) DOI: 10.3389/fpls.2016.00920.

Figures

Fig. 1. The wheat grain contains a cavity between the vascular tissue and the storage endosperm filled with a gel-like structure. Representative wheat grains and sections at 350 (A) and 550 (B) °DAF. All sections are transverse sections made in the equatorial part of the grain except for the right panel in B showing a longitudinal section from brush to embryo. Left side: macroscopic observations of fresh entire grains and sections. Right panels in (A), sections of wheat grains stained with the non-specific toluidine blue to highlight tissue organization (cryo-substituted sample with preserved cavity content). Middle panel in (B) sample cryo-sectioned sample without embedding and staining. Right panel in (A) and middle panel in (B): zoom on the endosperm cavity which contains a "gel" that does not leak during the sectioning process, is visible on thin cryo-sections and reacts with toluidine blue.

P: pericarp, e: endosperm, se: starchy endosperm, c: cavity, ne: nucellar epidermis, al: aleurone, tc: transfer cells, np: nucellar projection, vb: vascular bundle, emb: embryo, ch: chalaza. Scale bar: 1 mm except if indicated.

Fig. 2. The cavity content autofluoresces upon UV-light excitation and its fluorescence intensity profile resembles that of the nucellar epidermis and aleurone cell walls and of ferulic acid ester-linked to arabinose (FerAX). Fluorescence studies of wheat grain sections and reference compounds: representative images and fluorescence profiles. Grains were harvested, immediately freezed and cryo-sectioned. The sections were placed on quartz slides.

A Representative image acquired using a confocal microscope (BF bright-field and F fluorescence) showing the gel and its surrounding tissues. Right panel: fluorescence intensity profiles of samples at different stages of development (average value of three grain samples). The figure shows profiles obtained for the grain gel, nucellar epidermis cell walls (ne) and for control slides with no grain sample (sl)

B Fluorescence micrographs (representative images of sections of grains harvested at 450°DAF and of reference compounds). Fluorescence images were acquired using the TELEMOS microscope of the synchrotron SOLEIL under deep UV excitation (280 nm) and using 9 emission filters (spectral range indicated in the x axis in nm. Images correspond to the sum of intensity measured for all filters. They

show the fluorescence of the grain tissues (left), the cavity gel (middle), and ferulic acid ester-linked to arabinose. Lines: pixels selected for the fluorescence intensity extraction. Pseudospectra averaged for all selected pixels of wheat grain tissues, cavity content and reference compounds. The gel pseudospectra is similar to that of nucellus epidermis and to that of FerAX, but different from that of ferulic acid especially in the spectral range 370-410 nm.

Se: starchy endosperm, al: aleurone layer, ne: nucellar epidermis, tc: transfer cells, p: pericarp.

Fig. 3. The endosperm cavity contains hydroxycinnamic acids. (A) Images of the wheat endosperm cavity before and after laser-dissection of the gel (stage 650°DAF). (B) Chromatogram showing compounds released from dissected cavity content upon mild alkaline hydrolysis and separation on a C18 HPLC column combined with diode array detection. *p*-coumaric acid (pCA), ferulic acid (FA), and dimers of FA (diFA) were identified according to their retention time and absorption spectra by comparison with commercial FA and pCA and well-characterized samples (wheat aleurone, and maize bran). Peaks annotated with a star were shown to correspond to contaminant compounds from the dissection membrane.

Fig. 4. Fourier Transform-InfraRed spectroscopy revealed the presence of arabinoxylans (AX), proteins and starch in the wheat grain endosperm cavity. (A) Different types of spectra recorded in the cavity of cryo-sectioned grains. (B) Average spectra with major AX signals obtained at different stages of development with B1 showing the second derivative of the signal to highlight the peak attributed to low substituted AX and B2 showing a zoom on the peaks attributed to ferulic acid. (C) Spectra of purified and characterized AX fractions with contrasted levels of substitution with arabinose (A/X ratio) and C1 Second-derivative of the spectra showing specific peaks for low and high substitution (Robert et al., 2005).

Fig. 5. Xylan deposition in the developing wheat grain. Fluorescence micrographs of representative samples of wheat grains at different stages of development from flowering (0°DAF) to the onset of grain filling (200°DAF). Immunolabeling experiments were carried out using the antibody anti-AX1,

which recognizes xylans, on transverse sections collected at the equatorial region of the grain. The images show the central part of the grain sections. Arrows point at labeled structures. P: pericarp, np: nucellar projection, ne: nucellar epidermis, v: vascular tissue, e: endosperm, c: cavity, tc: transfer cells.

Fig. 6. Xylan detection in wheat grain at 200°DAF. Xylan epitopes are detected in cell walls, in intracellular vesicles, in the endosperm cavity and in the apoplast between the nucellar epidermis and the endosperm all around the grain. Micrographs of representative samples of wheat grain at 200°DAF. Immunolabelling experiments were carried out using the antibody anti-AX1, which recognizes xylans. Top: fluorescence micrographs. Arrows point at labelling within cells, buldging out cell walls and in intercellular spaces. Bottom: transmission electron micrographs showing immunogold detection as small dark dots in the nucellar epidermis walls, in intracellular vesicles, and in the endosperm cavity. P: pericarp, np: nucellar projection, ne: nucellar epidermis, v: vascular tissue, e: endosperm, c: cavity, tc: transfer cells.

Fig. 7. Microscopic Magnetic Resonance Imaging of the developing wheat grain. Transverse images obtained on representative grains at different stages: (A) 250°DAF, (B) 650°DAF and (C) 850°DAF. For each stage, eight contiguous slices are shown (numbered 1 to 8). For an example of complete wheat grain see figure S2. Images reveal the structure and water content of the grain. The color scale on the right indicates the normalized water content (in %).
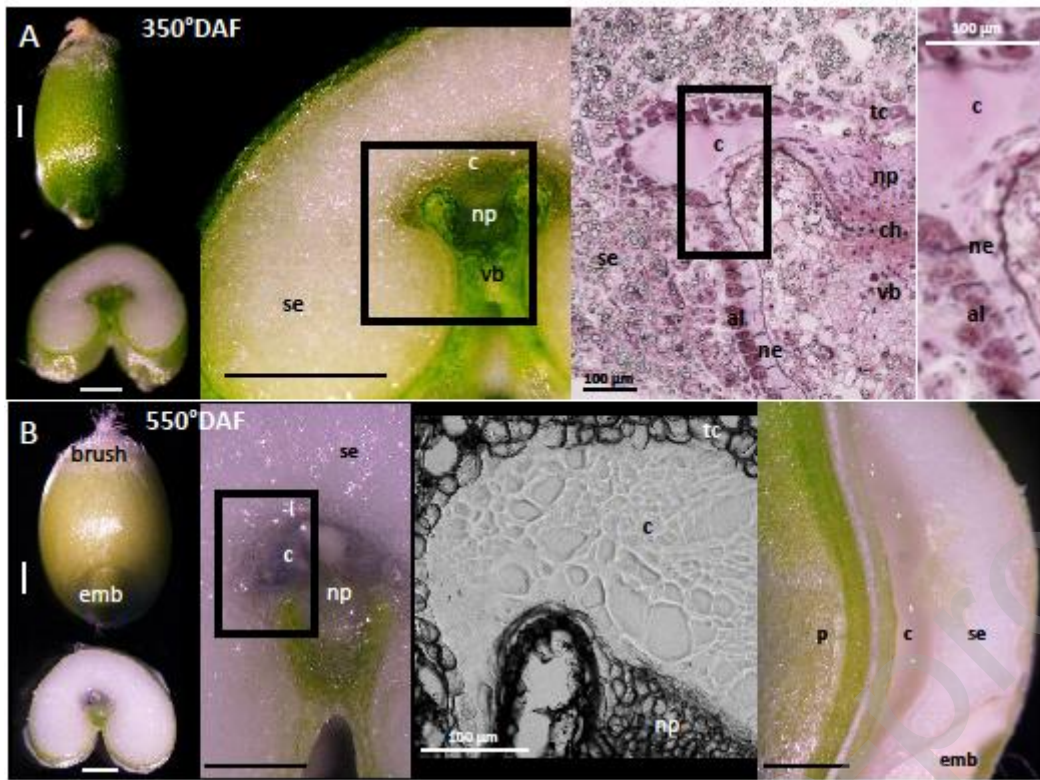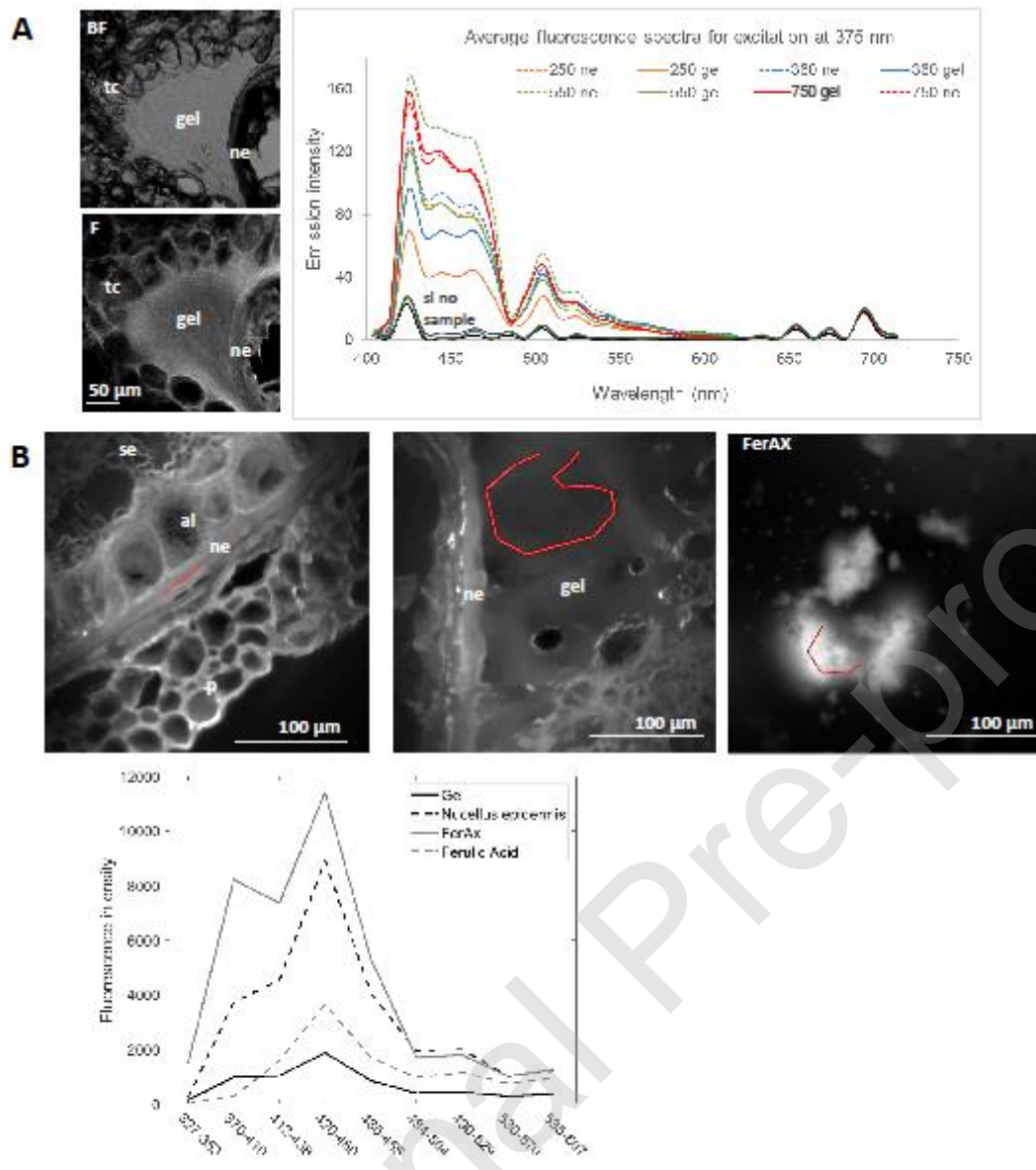
21
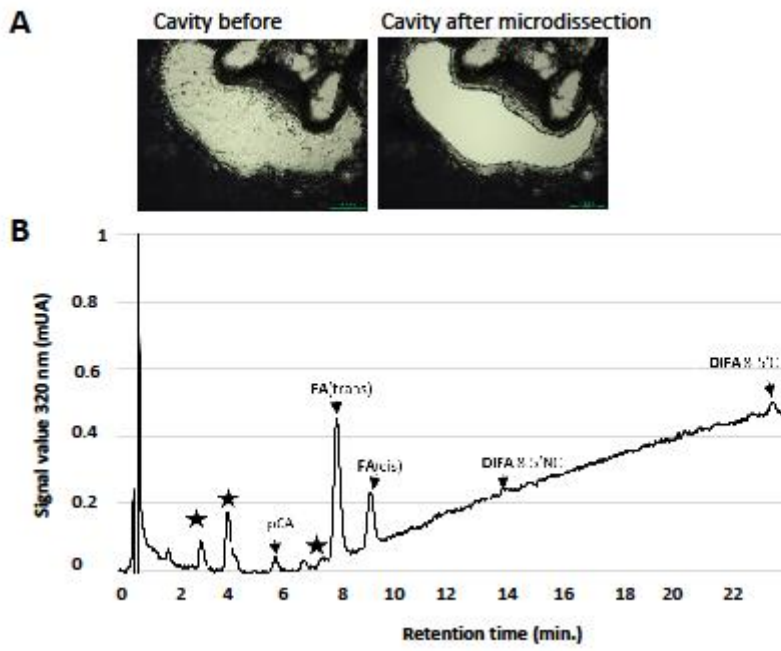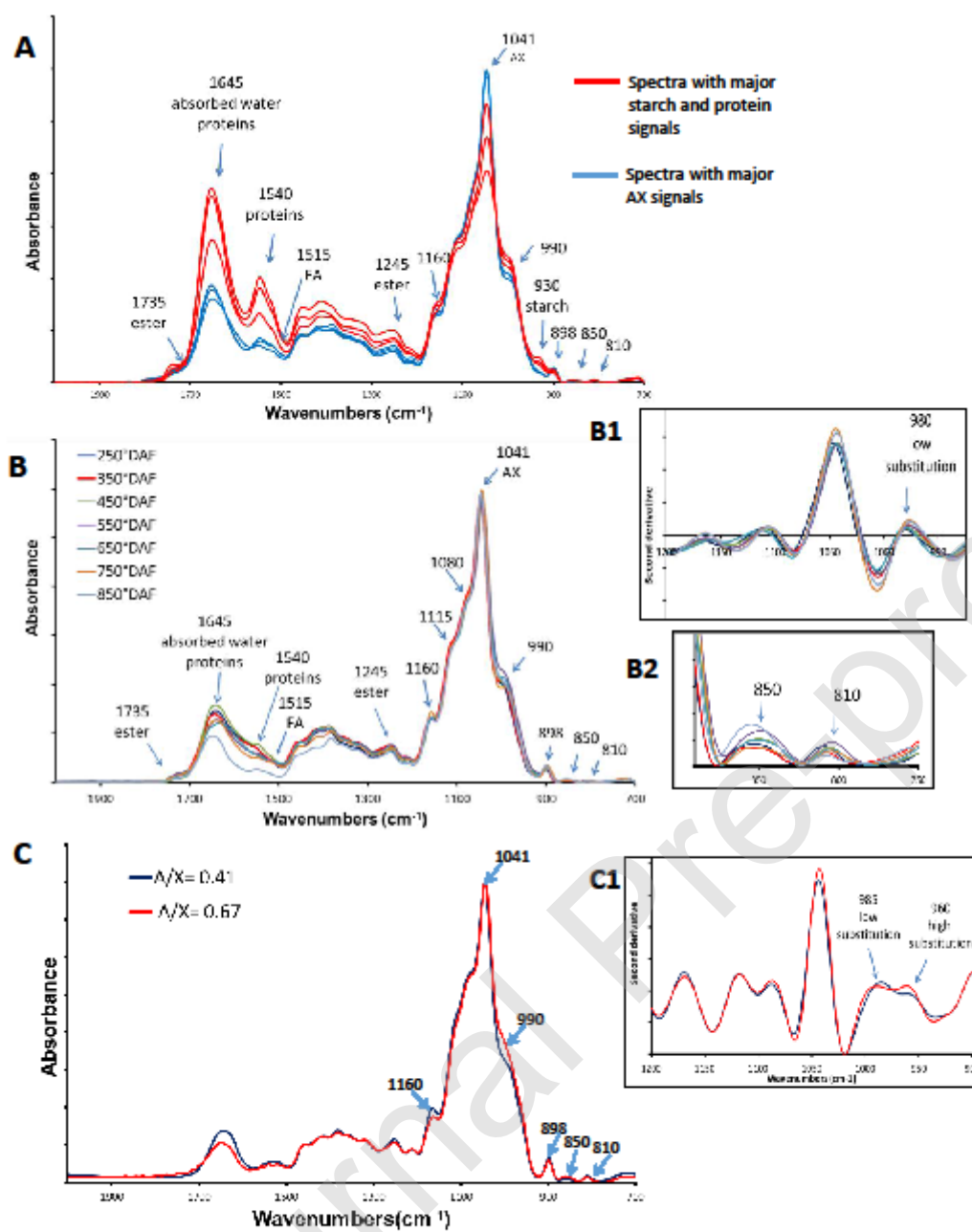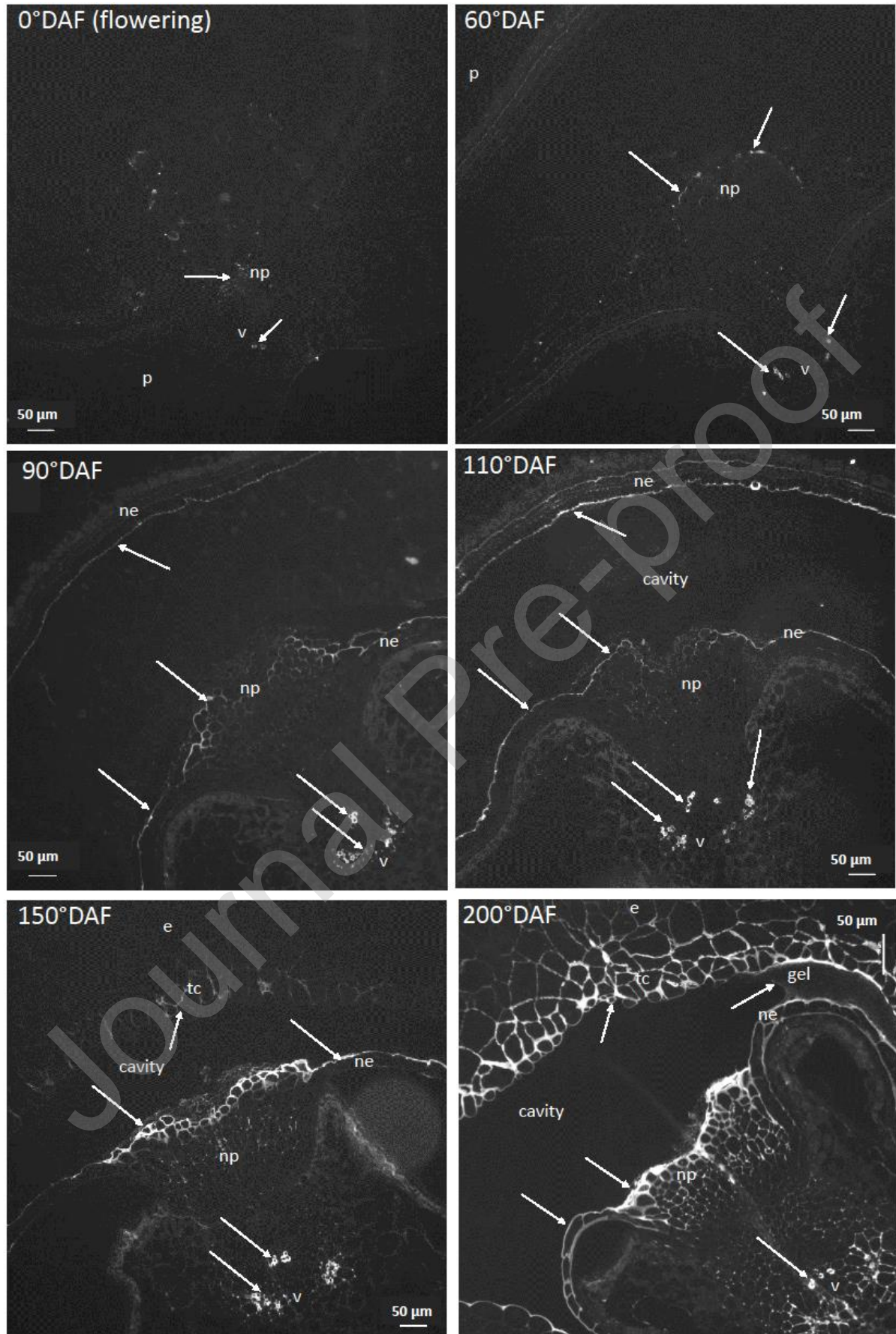
Fig 1

Fig. 1.

Fig 2

Fig. 2.

Fig 3

Fig. 3.

Fig 4

Fig. 4.

Fig 5
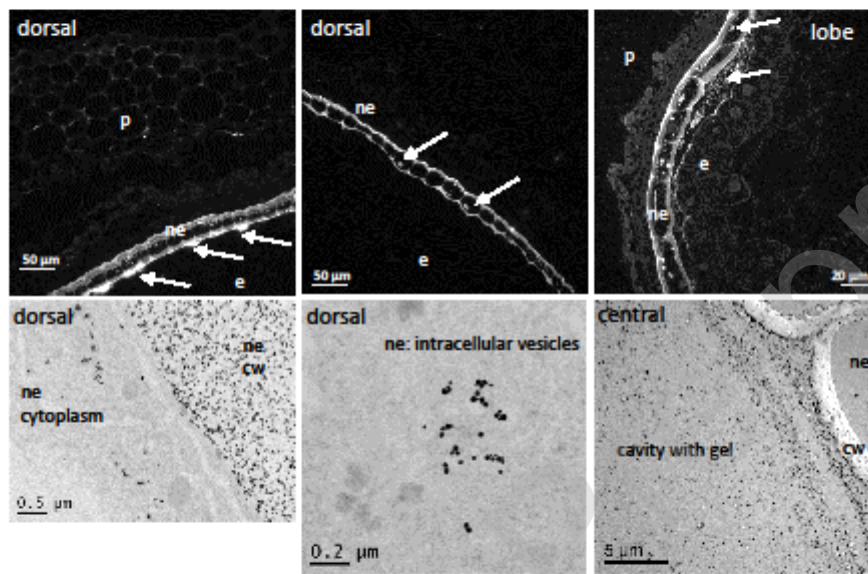

Fig. 5

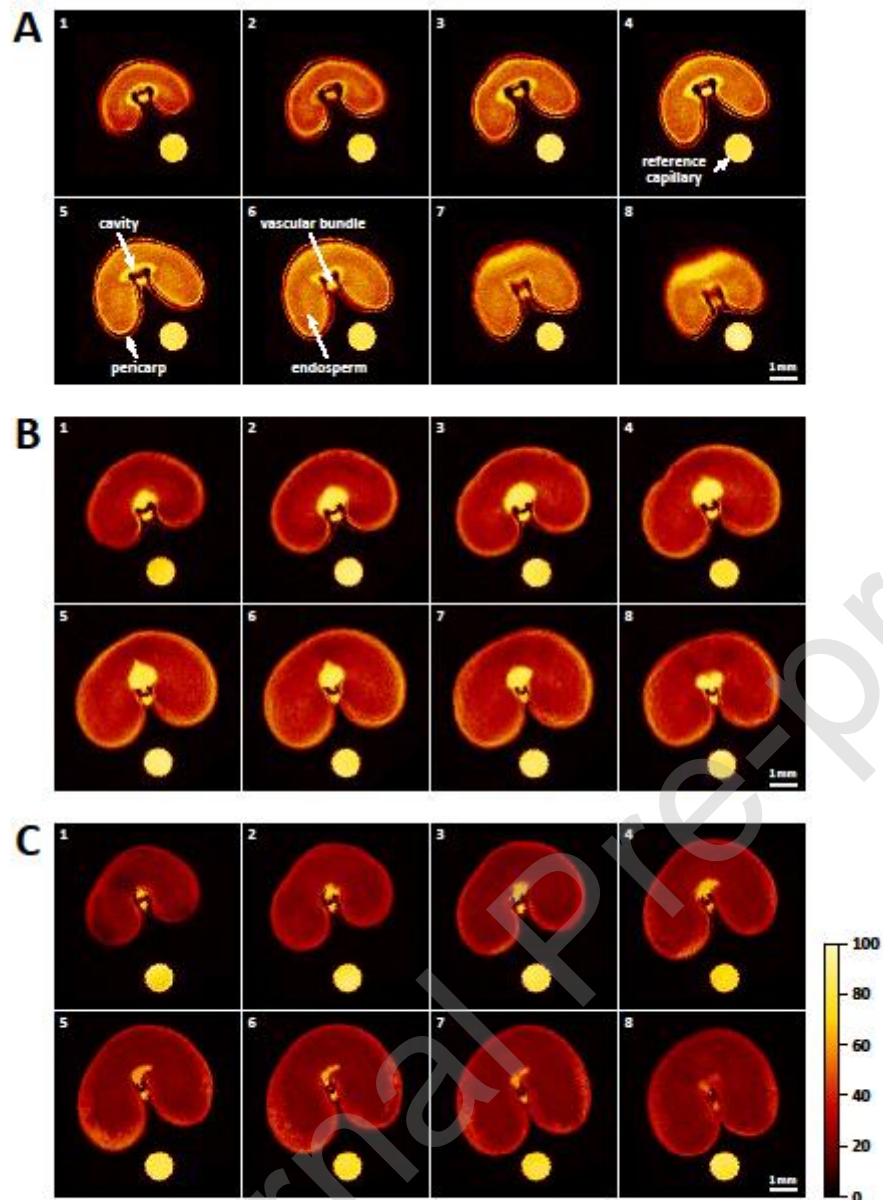Fig 6

Fig. 6

Fig 7

Fig. 7.

Table 1 Sample preparation, sectioning and acquisition settings for microscopy

Purpose	Sample preparation	Sectioning (transverse in equatorial region if not mentioned otherwise)	Section treatments	Microscope	Acquisition settings
Macroscopic observations whole grain Fig. 1	None	Scalpel (transverse & longitudinal)	None	Stereomicroscope SMZ800 Nikon, objective x1 plan apo WD70; camera Digital Sight DS-Fi2	Bright-field
Tissue organization Fig. 1	Cryo-substituted (high pressure freezing and substitution with Lowicryl HM20) [33]	Semi-thin sections (1 µm, ultracut UC7, Leica)	Toluidine blue staining	Multizoom macroscope AZ100M Nikon, objective x5 (zoom 8) AZ plan Fluor NA 0.5 WD 15; camera EXI Aqua QImaging 14 bits equipped with filter wheel RGB-HM-S-IR	Bright-field
Tissue organization: gel Fig. 1	None	Cryo-sections (30 µm); cryotome (HM500 OM, Microm)		Confocal laser scanning system A1 Nikon, objective x20 (zoom 2); transmitted light detector	Bright-field
UV-vis autofluorescence spectral imaging Fig S1	None	Cryo-sections (30 µm); cryotome (HM500 OM, Microm)	None	Microscope DMRD Leica, objective x10 plan Fluotar NA 0.3; camera Nikon DS-1QM 12 bits	Excitation (nm) band-pass 340–380 Emission (nm) > 425
Hyperspectral imaging Fig. 2A	None	Cryo-sections (30 µm); cryotome (HM500 OM, Microm)	None	Confocal laser scanning system A1 Nikon, equipped with a 32 channel PMT spectral detector unit; objective x20 (zoom 2) Emitted light collected from 400 to 720 nm	Excitation (nm) 375 Emission (nm) band-pass filter 425-475 414 to 704 (dichroic mirror)
Deep UV autofluorescence spectral imaging Fig. 2B	None	Cryo-sections (20 µm) cryotome (HM500 OM, Microm)	None	TELEMOS synchrotron SOLEIL Zeiss Axio Observer Z-1, objective x40; CCD camera Pixis BUV 16 bits Princeton instrument	Excitation (nm) 280 Multispectral acquisitions Emission filters (nm) : 1:327-353 ; 2: 370-410; 3: 412-438; 4: 420-480; 5: 435-455; 6: 484-504; 7: 499-529; 8: 530-570, 9: 535-607 5 sec for all filters
Cell wall polysaccharide immunodetection Fig. 5 and 6	Resin embedded LRWhite [23]	Semi-thin sections (1 µm; ultracut UC7, Leica)	Immuno-labelings	Microscope DMRD Leica, objective x20 plan Apo NA 0.6 and x40 plan Apo NA 0.75; camera Nikon DS-1QM 12 bits	Fluorescence [23] Excitation (nm) band-pass 515–560 Emission (nm) >590. For a given antibody, same time of exposure for all samples.
Cell wall polysaccharide immunodetection Fig. 6	Resin embedded LRWhite and cryo-substituted [23, 33]	Ultra-thin sections (80 nm, ultracut UC7, Leica)	Immuno-labelings	JEOL JEM 1230 transmission electron microscope; camera GATAN ES500W Erlangshen model 782	